

# Electronic properties of nanocrystalline $\text{LaNiO}_3$ and $\text{La}_{0.5}\text{Sr}_{0.5}\text{CoO}_3$ conductive films grown on silicon substrates determined by infrared to ultraviolet reflectance spectra

Z. G. Hu,<sup>1,a)</sup> W. W. Li,<sup>1</sup> Y. W. Li,<sup>1</sup> M. Zhu,<sup>2,b)</sup> Z. Q. Zhu,<sup>1</sup> and J. H. Chu<sup>1</sup>

<sup>1</sup>Key Laboratory of Polar Materials and Devices, Ministry of Education, East China Normal University, Shanghai 200241, People's Republic of China

<sup>2</sup>Department of Physics, Shanghai Jiao Tong University, Shanghai 200240, People's Republic of China

(Received 16 February 2009; accepted 13 May 2009; published online 1 June 2009)

Electronic band structures of nanostructured  $\text{LaNiO}_3$  (LNO) and  $\text{La}_{0.5}\text{Sr}_{0.5}\text{CoO}_3$  (LSCO) films have been investigated by near-normal incident optical reflectance at room temperature. Dielectric constants of the conductive films in the photon energy range of 0.47–6.5 eV have been extracted with the Drude–Lorentz function. It is found that four interband electronic transitions can be uniquely assigned for the perovskite-type metallic oxides. Moreover, optical conductivity is approximately varied from 100 to 450  $\Omega^{-1}\text{cm}^{-1}$  and shows a different variation trend for the LNO and LSCO layers. The discrepancy could be ascribed to diverse electronic structure, grain size, and crystalline formation. © 2009 American Institute of Physics. [DOI: 10.1063/1.3148339]

Ferroelectric (FE) polar film materials and devices have received much attention due to their potential technological applications in dynamic random access memories, electrooptic switches, pyroelectric detectors, and optical mixers.<sup>1,2</sup> Top and bottom electrodes play an important role in optoelectronic devices in order to deal with electrical and/or optical signal.<sup>3–6</sup> For example, polarization charges, which can be screened by free carriers inside the electrode, are induced at the electrode/FE interface in a FE-based capacitor. As we know,  $\text{LaNiO}_3$  (LNO) and  $\text{La}_{0.5}\text{Sr}_{0.5}\text{CoO}_3$  (LSCO), which are the highly conductive metallic oxides, have a distorted perovskite structure with a cubic lattice parameter of 3.84 and 3.83 Å, respectively.<sup>7–9</sup> As the matched electrodes for perovskite FE-based devices, LNO and LSCO materials have been widely studied as alternatives for platinum (Pt) and Pt-based metals.<sup>3,6,10</sup> It is because these metallic oxides can significantly improve the physical properties of FE devices, as compared with noble metal electrodes.<sup>10,11</sup> Therefore, understanding the intrinsic physical phenomena occurring within FE film and electrode/FE interface requires accurate knowledge of dielectric constants about the electrode.

Owing to an increasing interest of nanostructured FE materials and devices,<sup>12,13</sup> the physical properties of nanostructured electrodes should be further investigated in order to clarify the functionalities. In spite of the promising properties up to now,<sup>4,6,9</sup> there are no reports on dielectric function and optical conductivity of nanostructured LNO and LSCO materials, which can predicatively reflect the electrical transport properties and electronic band structure.<sup>14–16</sup> In particular, the optical and electronic properties could be remarkably different from the bulk crystal for LNO and LSCO materials with a low-dimensional structure.<sup>15</sup> Fortunately, optical reflectance technique can directly provide electronic band energy and dielectric constants. This makes it possible to investigate the optical function of nanostructured LNO and LSCO films in a wider photon energy range.<sup>4</sup> In this letter, the dielectric functions of nanostructured LNO and

LSCO films have been studied in the photon energy range of 0.47–6.5 eV. The discrepancy of optical conductivity and electronic transition has been discussed in detail.

Nanocrystalline LNO and LSCO films were deposited on the single-side polished silicon (Si) wafers by radio frequency magnetron sputtering and pulsed laser deposition methods, respectively.<sup>4,17</sup> The crystalline structures of the films were analyzed by x-ray diffraction (XRD) using  $\text{Cu } K\alpha$  radiation (D/MAX-2550V, Rigaku Co.) (see Fig. 1). It indicates that the films are crystallized with the single perovskite phase. Note that the LNO film presents a highly (100)-preferential orientation. Besides the strongest (110) peak, some weaker peaks (100), (111), (200), and (211) appear, indicating that the LSCO film is polycrystalline. According to the known Scherrer's equation, the grain size from the (200) and (110) peaks was evaluated to 78 and 27 nm for the LNO and LSCO films, respectively. The striking increment for the LNO film could be due to the better crystallization (i.e., highly preferential orientation).

Near-normal incident optical reflectance spectra ( $\sim 8^\circ$ ) were recorded at room temperature (RT) with a double beam ultraviolet infrared spectrophotometer (PerkinElmer Lambda 950) at the photon energy from 0.47 to 6.5 eV (190–2650 nm) with a spectral resolution of 2 nm. Aluminum (Al) mir-

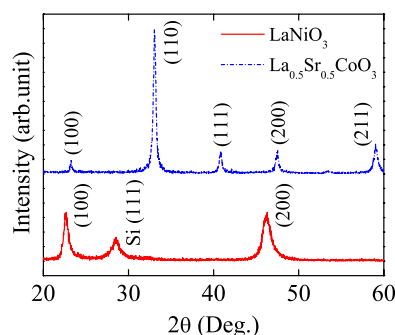


FIG. 1. (Color online) The XRD patterns of  $\text{LaNiO}_3$  and  $\text{La}_{0.5}\text{Sr}_{0.5}\text{CoO}_3$  films grown on Si substrates. Note that the (100) and (200) crystalline orientations are slightly different from the two samples.

<sup>a)</sup>Electronic mail: zghu@ee.ecnu.edu.cn.

<sup>b)</sup>Electronic mail: zhumin@sjtu.edu.cn.

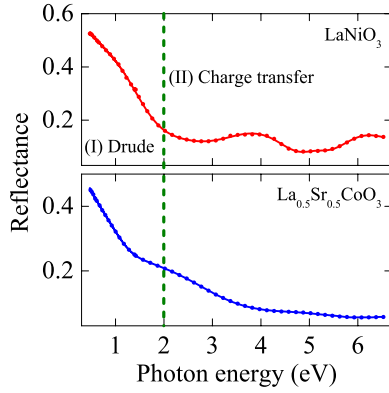


FIG. 2. (Color online) Experimental (dotted lines) and best-fit (solid lines) near-normal incident reflectance spectra of  $\text{LaNiO}_3$  and  $\text{La}_{0.5}\text{Sr}_{0.5}\text{CoO}_3$  films. The dashed line is applied to approximately distinguish two different electronic transition regions.

ror, whose absolute reflectance was directly measured, was taken as reference for the spectra in the photon energy region. It is noted that the nominal growth thickness is about 200 nm and 1  $\mu\text{m}$  for the LNO and LSCO films, respectively. Considering the light penetration depth in the samples due to the optical conductivity, a three-phase layered model (air/film/substrate) and the semi-infinite medium approach are applied to calculate the reflectance spectra of the LNO and LSCO films, respectively.<sup>4,18,19</sup> Owing to the conductivity of metallic oxide films, the dielectric function can be expressed using a Drude–Lorentz oscillator dispersion relation:  $\epsilon(E) = \epsilon_r + i\epsilon_i = \epsilon_\infty - (A_D/E^2 + iEB_D) + \sum_{j=1}^4 (A_j/E_j^2 - E^2 - iEB_j)$ .<sup>4,6,20</sup> Where  $\epsilon_\infty$  is the high-frequency dielectric constant,  $A_j$ ,  $E_j$ ,  $B_j$ , and  $E$  is the amplitude, center energy, broadening of the  $j$ th oscillator, and the incident photon energy, respectively. The experimental reflectance spectra of the LNO and LSCO films are shown in Fig. 2 with the dotted lines. Generally, the reflectance spectra recorded show the similar dependence on the photon energy except for the amplitude, which is slightly higher in the LNO film. Note that the reflectance spectrum from the LSCO film is similar to that of the film grown on MgO substrate, where a slight dip appears from optical reflectance measurement.<sup>21</sup>

The reflectance spectra can be roughly divided into two regions (see the dotted line in Fig. 2). The lower photon energy region below about 2 eV is assigned to a strong Drude response, which is derived from the intraband transition of free carrier. It was reported that the typical energy scale of the Jahn–Teller (JT) related excitations are varied between 0.5 and 3 eV.<sup>22</sup> It indicates that the  $\text{Ni}^{3+}$  and  $\text{Co}^{3+}$  ions related JT effect is important in the perovskite-type materials, whose lattice distortion can couple via an orbital exciton strongly in the  $3d$  correlated metallic systems.<sup>14</sup> The results are similar to some high temperature superconductors.<sup>22</sup> The charge-transfer excitations are located above 2.0 eV for the LNO and LSCO films. The interband electronic transitions are mainly derived from O  $2p$  and Ni/Co  $3d$  energy states.<sup>15</sup> It was argued that the crystal field splitting and the JT effect in the metallic oxides can affect the charge-transfer transitions.<sup>22</sup> In order to clarify the different transition energy bands, the Lorentz oscillator model expressing the respective contribution to the optical response is necessary. The reproduced optical reflectance results with the Drude–Lorentz model are also shown in Fig. 2 by the solid

TABLE I. The Lorentz oscillator parameter values of  $\text{LaNiO}_3$  and  $\text{La}_{0.5}\text{Sr}_{0.5}\text{CoO}_3$  films are determined from the simulation of reflectance spectra in Fig. 2. The 90% reliability of the fitting parameters is given with ( $\pm$ ).

		$A_j$ (eV) <sup>2</sup>	$E_j$ (eV)	$B_j$ (eV)
$\text{LaNiO}_3$	$j=1$	$1.97 \pm 0.09$	$2.32 \pm 0.02$	$2.28 \pm 0.05$
	$j=2$	$2.0 \pm 0.1$	$3.36 \pm 0.01$	$2.16 \pm 0.06$
	$j=3$	$0.19 \pm 0.01$	$5.10 \pm 0.02$	$0.9 \pm 0.1$
	$j=4$	$2.69 \pm 1.07$	$7.31 \pm 0.41$	$3.29 \pm 0.93$
$\text{La}_{0.5}\text{Sr}_{0.5}\text{CoO}_3$	$j=1$	$0.33 \pm 0.06$	$1.55 \pm 0.01$	$1.22 \pm 0.06$
	$j=2$	$2.31 \pm 0.06$	$2.11 \pm 0.04$	$3.06 \pm 0.06$
	$j=3$	$1.57 \pm 0.07$	$4.59 \pm 0.01$	$3.03 \pm 0.07$
	$j=4$	$0.10 \pm 0.02$	$6.01 \pm 0.03$	$0.73 \pm 0.10$

lines and the parameter values are given in Table I. Note that the thickness of the LNO film is estimated to  $235 \pm 1$  nm, which is slightly larger than the nominal growth value. It should be emphasized that the present optical stacking models for the LNO and LSCO films can be accepted due to the reasonable fitting values and their standard errors. In particular, the oscillator broadening are generally less than the corresponding  $E_j$  values (see Table I), indicating that the Drude–Lorentz dispersion is reliable and satisfying, similar to the results from some metal films.<sup>5</sup>

It is testified that four Lorentz oscillators are requisite for the nanocrystalline films, as compared with some noble metal films.<sup>5</sup> These Lorentz oscillators can correspond to different interband electronic transitions, respectively. For the LNO material, the optical transition peaks are located at  $2.32 \pm 0.02$ ,  $3.36 \pm 0.01$ ,  $5.10 \pm 0.02$ , and  $7.31 \pm 0.41$  eV. These center energy positions can be readily distinguished from the reflectance spectrum. For the LSCO film, however, the four center energy peaks are found at  $1.55 \pm 0.01$ ,  $2.11 \pm 0.04$ ,  $4.59 \pm 0.01$ , and  $6.01 \pm 0.03$  eV, respectively. Compared with the result of the LNO film, these transition energy positions are overlapped on the reflectance spectrum due to the large broadening. As compared with the theoretical model of the band structure for the metallic oxides,<sup>22–24</sup> the four energy bands can be assigned to the following electronic transitions: (1) O  $2p$  to Ni/Co  $3d$  ( $t_{2g}$ –JT); (2) O  $2p$  to Ni/Co  $3d$  ( $t_{2g}$ +JT); (3) O  $2p$  to Ni/Co  $3d$  ( $e_g$ –JT); and (4) O  $2p$  to Ni/Co  $3d$  ( $e_g$ +JT), respectively. The results are in good agreement with the data from the photoemission spectroscopy, in which four prominent band structures can be observed above the Fermi level ( $E_F$ ).<sup>15</sup> Based on the Drude model parameters, it can be found that the plasma frequency of the LSCO film ( $A_D$  is  $3.47 \pm 0.04$  eV) is slightly larger than that from the LNO film ( $A_D$  is  $3.34 \pm 0.03$  eV). Note that the parameter  $B_D$  is  $0.74 \pm 0.01$  eV and  $0.84 \pm 0.01$  eV for the LNO and LSCO films, respectively. The phenomena can be confirmed from the reflectance spectra.

From the model parameters, the dielectric constants can be readily obtained. The evolution of  $\tilde{\epsilon}(E)$  with the photon energy for the LNO and LSCO films is shown in Figs. 3(a) and 3(b). Generally, the real part  $\epsilon_r$  increases with the photon energy and the values for LNO and LSCO films are evaluated to be about  $-3.3$  and  $-2.5$  at 0.47 eV, respectively. Note that the  $\epsilon_r$  of the LSCO film is slightly larger than that of the LNO film in the mid-infrared region. According to the Drude model, the free carrier results in the fact that the dielectric constant decreases to a high negative value as photon

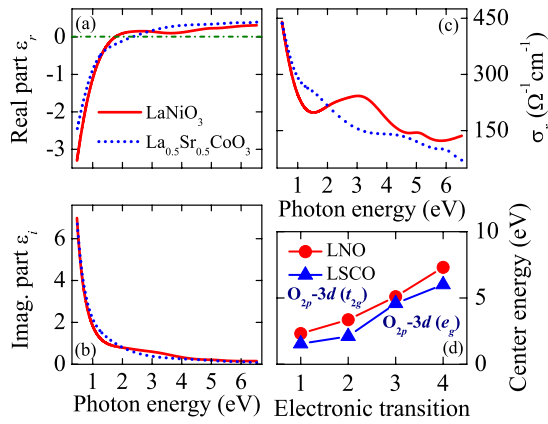


FIG. 3. (Color online) The real part (a) and imaginary part (b) of dielectric function in  $\text{LaNiO}_3$  and  $\text{La}_{0.5}\text{Sr}_{0.5}\text{CoO}_3$  films from infrared to ultraviolet photon energy regions. The comparison of the optical conductivity between two films (c) and (d) the Lorentz oscillator  $E_j$  value corresponds to the electronic transitions from O  $2p$  to Ni/Co  $3d$ , respectively.

energy approaches zero.<sup>5</sup> It indicates that the contribution from the Drude response becomes more prominent for the LSCO material, which agrees well with the above analysis on the plasma frequency. On the other hand, the imaginary part  $\epsilon_i$  strikingly decreases with the photon energy and approaches zero toward the ultraviolet energy region, indicating the contributions from the strong interband transitions. Note that the  $\epsilon_i$  is slightly smaller than those of noble metal films. The  $\epsilon_i$  discrepancy between the LNO and LSCO films is not obvious, as compared with the  $\epsilon_r$ . It can be attributed to the fact that they have the similar perovskite crystalline structure.

In order to give a further insight on the electronic structure of the LNO and LSCO films, the real part of optical conductivity  $\sigma$  can be calculated by  $\sigma_r = \epsilon_0 \omega \epsilon_i$ , here  $\epsilon_0$  and  $\omega$  is the vacuum dielectric constant and the light frequency, respectively. Figure 3(c) gives a comparison of the  $\sigma_r$  for the LNO and LSCO films. Although the  $\sigma_r$  is approximately varied from 100 to  $450 \text{ } \Omega^{-1} \text{ cm}^{-1}$ , the optical conductivity presents a different behavior for the perovskite-type oxide materials. In the midinfrared region, the  $\sigma_r$  rapidly increases with decreasing photon energy because of the contribution from the Drude response. Then the optical conductivity rapidly decreases with further increasing the photon energy. From the visible to ultraviolet energy regions, the absorption peaks owing to the interband electronic transitions can be easily distinguished for the LNO film, compared with the LSCO film. Note that the conductive behavior for the two samples is similar to those of high-temperature superconductivity.<sup>21</sup>

Figure 3(d) shows the four energy bands for the charge-transfer excitations. Considering the corresponding electronic structure, the transition energy of the LNO film is slightly larger than those of the LSCO film. The small discrepancy is mainly due to Ni or Co  $3d$  electronic states for the LNO and LSCO materials, respectively. Owing to the distinct  $3d$  orbital energy, the  $t_{2g}$  and  $e_g$  states can be located at different level in the energy space, which induces the center energy variation for two perovskite-type oxides. Note that the La and/or Sr composition ratio can affect the O  $2p$  and  $3d$  orbital distributions as well.<sup>22</sup> It was reported that the structural distortions can affect the electronic band structures of the perovskite material.<sup>24,25</sup> Therefore, the highly preferential

orientation LNO and polycrystalline LSCO layers can contribute to the changed electronic structure. In addition, the LNO and LSCO films have different grain size, which results in the grain boundary discrepancy and maybe further affect the electronic state.

In conclusion, the dielectric functions of high-quality LNO and LSCO conductive oxide films have been investigated by fitting the reflectance spectra with the Drude-Lorentz model. The optical conductivity presents a different behavior for two perovskite-type oxides due to the contributions from the charge-transfer excitations.

This work was financially sponsored by Major State Basic Research Development Program of China (Grant No. 2007CB924901), the Program of New Century Excellent Talents, MOE (Grant No. NCET-08-0192), Shanghai Municipal Commission of Science and Technology Project (Grant Nos. 07JC14018, 07DZ22943, 08JC1409000, and 08520706100).

- <sup>1</sup>C. H. Ahn, K. M. Rabe, and J.-M. Triscone, *Science* **303**, 488 (2004).
- <sup>2</sup>J. F. Scott, *Science* **315**, 954 (2007).
- <sup>3</sup>B. Yang, S. Aggarwal, A. M. Dhote, T. K. Song, R. Ramesh, and J. S. Lee, *Appl. Phys. Lett.* **71**, 356 (1997).
- <sup>4</sup>Z. G. Hu, Z. M. Huang, Y. N. Wu, Q. Zhao, G. S. Wang, and J. H. Chu, *J. Appl. Phys.* **95**, 4036 (2004).
- <sup>5</sup>W. S. Choi, S. S. A. Seo, K. W. Kim, T. W. Noh, M. Y. Kim, and S. Shin, *Phys. Rev. B* **74**, 205117 (2006).
- <sup>6</sup>B. Berini, N. Keller, Y. Dumont, E. Popova, W. Noun, M. Guyot, J. Vigneron, A. Etcheberry, N. Franco, and R. M. C. da Silva, *Phys. Rev. B* **76**, 205417 (2007).
- <sup>7</sup>C. Rossel, A. Rosová, K. Hušková, D. Machajdík, and K. Fröhlich, *J. Appl. Phys.* **100**, 044501 (2006).
- <sup>8</sup>C. K. Xie, J. I. Budnick, B. O. Wells, and J. C. Woicik, *Appl. Phys. Lett.* **91**, 172509 (2007).
- <sup>9</sup>W. Noun, B. Berini, Y. Dumont, P. R. Dahoo, and N. Keller, *J. Appl. Phys.* **102**, 063709 (2007).
- <sup>10</sup>G. P. Mambri, E. R. Leite, M. T. Escote, A. J. Chiquito, E. Longo, J. A. Varela, and R. F. Jardim, *J. Appl. Phys.* **102**, 043708 (2007).
- <sup>11</sup>M. Angadi, O. Auciello, A. R. Krauss, and H. W. Gundel, *Appl. Phys. Lett.* **77**, 2659 (2000).
- <sup>12</sup>I. I. Naumov, L. Bellaiche, and H. Fu, *Nature (London)* **432**, 737 (2004).
- <sup>13</sup>J. Kim, S. A. Yang, Y. C. Choi, J. K. Han, K. O. Jeong, Y. J. Yun, D. J. Kim, S. M. Yang, D. Yoon, H. Cheong, K.-S. Chang, T. W. Noh, and S. D. Bu, *Nano Lett.* **8**, 1813 (2008).
- <sup>14</sup>K. Sreedhar, J. M. Honig, M. Darwin, M. McElfresh, P. M. Shand, J. Xu, B. C. Crooker, and J. Spalek, *Phys. Rev. B* **46**, 6382 (1992).
- <sup>15</sup>K. Horiba, R. Eguchi, M. Taguchi, A. Chainani, A. Kikkawa, Y. Senba, H. Ohashi, and S. Shin, *Phys. Rev. B* **76**, 155104 (2007).
- <sup>16</sup>P. L. Kuhns, M. J. R. Hoch, W. G. Moulton, A. P. Reyes, J. Wu, and C. Leighton, *Phys. Rev. Lett.* **91**, 127202 (2003).
- <sup>17</sup>Y. W. Li, Z. G. Hu, F. Y. Yue, W. Z. Zhou, P. X. Yang, and J. H. Chu, *Appl. Phys. A: Mater. Sci. Process.* **95**, 721 (2009).
- <sup>18</sup>O. S. Heaven, *Optical Properties of Thin Solid Films* (Dover, New York, 1991).
- <sup>19</sup>Z. G. Hu, A. G. U. Perera, Y. Paltiel, A. Raizman, and A. Sher, *J. Appl. Phys.* **98**, 023511 (2005).
- <sup>20</sup>M. M. Qazilbash, A. A. Schafgans, K. S. Burch, S. J. Yun, B. G. Chae, B. J. Kim, H. T. Kim, and D. N. Basov, *Phys. Rev. B* **77**, 115121 (2008).
- <sup>21</sup>I. Bozovic, J. H. Kim, J. S. Harris, Jr., C. B. Eom, J. M. Phillips, and J. T. Cheung, *Phys. Rev. Lett.* **73**, 1436 (1994).
- <sup>22</sup>A. Rusydi, R. Rauer, G. Neuber, M. Bastjan, I. Mahns, S. Müller, P. Saichu, B. Schulz, S. G. Singer, A. I. Lichtenstein, D. Qi, X. Gao, X. Yu, A. T. S. Wee, G. Stryganyuk, K. Dörr, G. A. Sawatzky, S. L. Cooper, and M. Rübhausen, *Phys. Rev. B* **78**, 125110 (2008).
- <sup>23</sup>S. R. Barman, A. Chainani, and D. D. Sarma, *Phys. Rev. B* **49**, 8475 (1994).
- <sup>24</sup>A. Yu. Dobin, K. R. Nikolaev, I. N. Krivorotov, R. M. Wentzcovitch, E. D. Dahlberg, and A. M. Goldman, *Phys. Rev. B* **68**, 113408 (2003).
- <sup>25</sup>Z. G. Hu, Y. W. Li, F. Y. Yue, Z. Q. Zhu, and J. H. Chu, *Appl. Phys. Lett.* **91**, 221903 (2007).